PCCP

Hydride- and Halide-Substituted Au9(PPh3)83+ Nanoclusters: Similar Absorption Spectra Disguise Distinct Geometries and Electronic Structures

Journal:	*Physical Chemistry Chemical Physics*
Manuscript ID	CP-ART-06-2021-002761.R1
Article Type:	Paper
Date Submitted by the Author:	27-Jul-2021
Complete List of Authors:	Ceylan, Yavuz; Brandeis University, Department of Chemistry Gieseking, Rebecca; Brandeis University, Department of Chemistry

Hydride- and Halide-Substituted $Au_9(PH_3)_8^{3+}$ Nanoclusters: Similar Absorption Spectra Disguise Distinct Geometries and Electronic Structures

Yavuz S. Ceylan, Rebecca L. M. Gieseking*

Department of Chemistry, Brandeis University

415 South Street, Waltham, Massachusetts 02453

* Corresponding author: gieseking@brandeis.edu; (781)-736-2511

Abstract

Ligands dramatically affect the electronic structure of gold nanoclusters (NCs) and provide a useful handle to tune the properties required for nanomaterials that have high performance for important functions like catalysis. Recently, questions have arisen about the nature of the interactions of hydride and halide ligands with Au NCs: hydride and halide ligands have similar effects on the absorption spectra of Au_9 NCs, which suggested that the interactions of the two classes of ligands with the Au core may be similar. Here, we elucidate the interactions of halide and hydride ligands on phosphine-protected gold clusters via theoretical investigations. The computed absorption spectra using time-dependent density functional theory are in reasonable agreement with the experimental spectra, confirming that the computational methods are capturing the ligand-metal interactions accurately. Despite the similarities in the absorption spectra, the hydride and halide ligands have distinct geometric and electronic effects. The hydride ligand behaves as a metal dopant and contributes its two electrons to the number of superatomic electrons, while the halides act as electron-withdrawing ligands and do not change the number of superatomic electrons. Clarifying the binding modes of these ligands will aid in future efforts to use ligand derivatization as a powerful tool to rationally design Au NCs for use in functional materials.

1. Introduction

Atomically precise noble metal nanoclusters (NCs) composed of a metal core surrounded by ligands have been studied widely in recent years for their catalytic activity for industrially important reactions,[1–8] particularly as photocatalysts.[9–13] Although gold nanoparticles and nanostructures have plasmonic properties that reflect a continuum of electronic states, gold NCs with diameters less than a few nm have discrete orbital energies and exciton-like excited-state properties.[14,15] For this reason, gold NCs often have higher photocatalytic activity than larger nanoparticles.[16,17] Tuning the electronic structures of gold NCs is a critical way to control their catalytic activity.[8,18] The precise structural control of noble metal NCs has enabled detailed study of catalytic reaction mechanisms[19,20] and elucidation of the active sites,[21–23] as well as investigation of the effects of structural changes as small as single atoms.[22,24–26]

Ligands play a critical role in determining the electronic structure and catalytic activity of Au NCs. The ligands dramatically affect many properties, including which NC sizes are stable, the geometric structure of the Au core, and the NC electronic structure.[27,28] Ligand substitution can dramatically change the activity and selectivity of catalytic reactions,[29–31] as well as the reaction mechanism.[32] Deliberate choice of ligand shapes[33] and ligand-metal bond strengths[34] can promote the formation of undercoordinated metal atoms that act as active sites for catalysis. Thus, understanding the connection between the choice of ligand, the NC size and geometry, and the chemical properties of the resulting NCs is a necessary step toward designing NCs with properties that are tuned to enhance their catalytic or photocatalytic activity.[30,35–38] A detailed understanding

of the geometric and electronic properties of the ligands is key to developing structure/function relationships in NC-based nanomaterials.

Several classes of ligands have been shown to have different binding modes and electronic effects on Au NCs. Thiolate ligands typically form "staple" motifs (-SR-Au-SR- or similar) on the NC surface; in contrast, alkene, phosphine, and halide ligands typically bind directly to the Au core.[39] The electronic effects of the ligands are also quite distinct. The electronic structure of Au NCs can be understood in terms of a superatomic model,[40–42] which has been widely used to understand and predict NC properties.[43–50] In this model, the Au valence orbitals (6s and 6p) create superatomic molecular orbitals (MOs) that are delocalized across the metal core with shapes that resemble those of atomic orbitals (1S, 1P, 1D, 2S, etc.); 'magic number' occupations that correspond to filled superatomic shells have high stability. A bare, neutral Au NC has one superatomic electron per Au atom. Ligands such as thiolates and halides typically act as electron-withdrawing ligands, and each ligand reduces the number of electrons in the superatomic Au core by one; in contrast, weaker ligands like phosphines do not modify the number of superatomic electrons in the Au core.[40]

Hydride ligands have been of particular interest in recent years because of their unique interactions with the Au NC. Binding of hydrogen to NCs is a critical step in catalysis of reactions such as hydrogen evolution,[51] and some Au NCs bind hydrogen more strongly than well-known Pt catalysts.[52] Early photoelectron experiments suggested that hydrogen atoms behave like monovalent metal atoms when adsorbed on bare Au NCs;[53] these results were supported by DFT calculations of the electronic structures of similar NCs.[54] Based on these results, the hydride ligand has been described as a metal dopant rather than as a traditional ligand. In recent years, this

description of hydrogen as a metal dopant has been extended to ligand-protected Au NCs based on both computational[55–57] and experimental[55,56,58] evidence. Unlike typical electron-withdrawing and weak ligands, the two electrons of the hydride are added to the superatomic electron count, increasing the total number of electrons in superatomic orbitals.

The $Au_9(PPh_3)_8^{3+}$ NC is an accessible platform to understand the behavior of ligands. $Au_9(PPh_3)_8^{3+}$ was one of first Au NCs synthesized and is accessible in gram-scale quantities,[59] and the NC has been widely studied using both experimental and theoretical tools.[44,56,58,60,61] Two distinct geometries of the NC have been observed in crystal structures, depending on the choice of anion and solvent: the metal core may have either approximate D_{4d} symmetry[62] or approximate D_{2h} symmetry.[63,64] In both geometries, the central Au atom is bonded only to eight outer Au atoms, making it a low-coordination site that is accessible as a binding site for an additional hydride ligand.[55] In the gas phase, this NC can undergo collision-induced interconversion between forms with different effective sizes.[65]

Recently, Johnson et al. produced new experimental evidence that called into question the previously accepted assignments of hydrides as metal dopants and halides as electron-withdrawing ligands.[66] Using a technique that couples mass spectroscopy to electronic absorption spectra, they showed that the $Au_9(PPh_3)_8H^{2+}$, $Au_9(PPh_3)_8Cl^{2+}$, and $Au_9(PPh_3)_8Br^{2+}$ NCs have surprisingly similar gas-phase absorption spectra (**Figure 1**). The unsubstituted $Au_9(PPh_3)_8^{3+}$ NC (**Figure 1a**) has five distinct absorption peaks between 2.4 and 3.4 eV, and the central peak near 2.9 eV has an intensity more than twice that of any of the other peaks. In contrast, all three ligand-substituted NCs (**Figure 1b-d**) have absorption spectra that exhibit plateaus across at least a 0.5 eV range.

This plateau extends from 2.6-3.3 eV for the hydride-substituted cluster, 2.5-3.1 eV for the chloride-substituted cluster, and 2.5-3.0 eV for the bromide-substituted cluster. Johnson et al. proposed that the similarities in the absorption spectra are due to similarities in the electronic structures of the ligand-substituted NCs: either hydride, chloride, and bromide all behave as metal dopants, or all three ligands are all electron-withdrawing. Either of these interpretations would substantially modify the current model of ligand behavior in Au NCs.

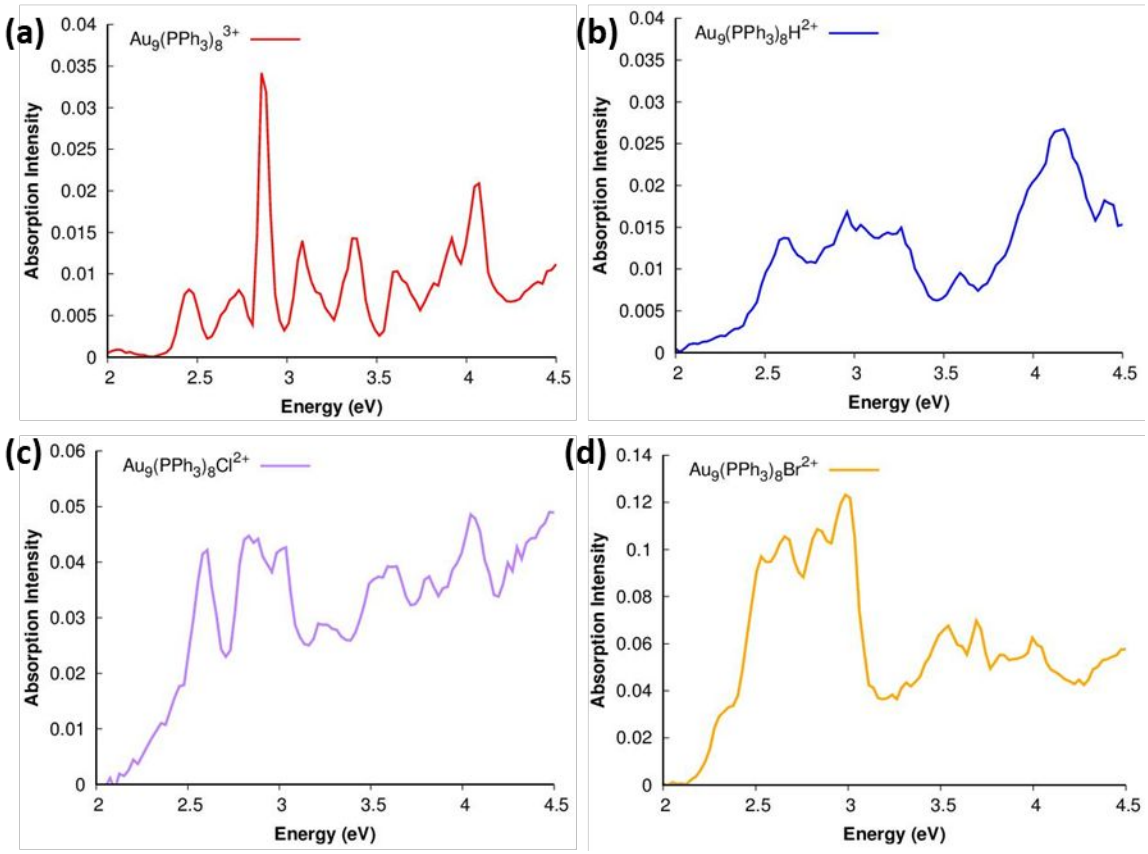

Figure 1. Experimental absorption spectra of (a) $Au_9(PPh_3)_8^{3+}$, (b) $Au_9(PPh_3)_8H^{2+}$, (c) $Au_9(PPh_3)_8Cl^{2+}$, and (d) $Au_9(PPh_3)_8Br^{2+}$. Data is from ref.[66]

Here, we examine the unsubstituted $Au_9(PPh_3)_8^{3+}$ NC and the hydride- and halide-substituted NCs using density functional theory (DFT) to understand the effect of the ligands on the NC geometric

and electronic structures and absorption spectra. We focus in particular in clarifying the binding modes of the two classes of ligands and directly comparing our computed absorption spectrum to the experimental spectra of the same NCs. We show that the superficially similar absorption spectra in these NCs occur despite substantial differences in the geometric and electronic structures. Instead, the hydride-substituted NC has properties that suggest that the hydride ligand is a metal dopant that binds to the central Au atom, consistent with previous theoretical results. In contrast, the halide ligands behave like electron-withdrawing ligands and unexpectedly bind in a bridging position to two outer Au atoms. These results highlight the importance of detailed theoretical study to elucidate the properties of Au NCs.

2. Computational Methods

The geometries of the Au NCs were optimized using a multi-step process. Our initial geometries were based on symmetrized versions of the D_{4d}[63] and D_{2h}[64] crystal structures of $Au_9(PH_3)_8^{3+}$, with the experimental PPh_3 ligands replaced with PH_3 to reduce computational cost. Starting from each geometry, we constructed eleven different structures of each ligand-protected Au NC with different initial positions of the hydride or halide ligand, including structures with the ligand near the central Au atom and structures with the ligand near the outer Au atoms. The initial optimizations were performed using the BP86 functional[67,68] and a double-ζ (DZ) Slater-type basis set with a frozen-core approximation for the Au 1s-5p orbitals; the BP86 function has been widely used for Au NCs[69–72] and is a low computational cost GGA-type functional. In a second step, for each ligand-substituted NC, all distinct local minima with energies less than 10.0 kcal/mol higher than the most stable structure were re-optimized using the revTPSS[73] functional with a triple-ζ

polarized (TZP) Slater-type all-electron basis set. In previous benchmarking studies, the revTPSS functional has performed particularly well for the relative energies and geometries of Au NCs.[74] The geometries of the PPh_3-ligated clusters were constructed based on the most stable PPh_3-ligated structures after replacing the PH_3 ligands with PPh_3 ligands, and likewise optimized using the revTPSS functional with a triple-ζ polarized (TZP) Slater-type all-electron basis set.

For all PH_3-ligated NCs within 11.9 kcal/mol of the most stable structure in the revTPSS optimizations and for all PPh_3-ligated NCs, the excited states in dipole-allowed symmetry groups were computed using a time-dependent DFT (TD-DFT) approach with the SAOP functional[75] and TZP all-electron basis set. For reasons of computational cost, the lowest 200 excited states of the PH_3-ligated NCs and the lowest 100 excited states of the PPh_3-ligated NCs were computed. Relativistic effects were incorporated using the zeroth-order regular approximation (ZORA)[76] in both ground and excited state calculations. We note that spin-orbit corrections are not included in these calculations. Although spin-orbit coupling may improve the computed absorption spectra to give more quantitative agreement with the experimental spectra,[77,78] its computational cost is prohibitive for these systems, and qualitative agreement is sufficient to show the electronic effects of the ligands. All calculations were performed using the Amsterdam Density Functional (ADF) 2018 software package.[79,80]

The absorption spectra were simulated by applying a Lorentzian broadening to the TD-DFT stick spectrum with a full width at half maximum (FWHM) of 0.0087 a.u. To compute the superatomic contributions to the absorption spectra, we visually identified the occupied molecular orbitals (MOs) with superatomic character. The superatomic character of each excited state was computed

as the weighted percentage of the excitations contributing to the state that involve superatomic occupied MOs, consistent with our previous definitions.[81] The superatomic contributions to the absorption spectra were computed by scaling the oscillator strength of each excited state by its superatomic character.

3. Results

Because the binding modes of the ligands can significantly affect the NC properties, we examine the effects of hydride and halide ligands on the $Au_9(PH_3)_8^{3+}$ and $Au_9(PPh_3)_8^{3+}$ NCs to clarify the binding modes of the ligands and reveal their effect on the NC absorption spectra. We first examine the unsubstituted $Au_9(PPh_3)_8^{3+}$, which has been widely studied experimentally and computationally;[44,56,58,60,61] our results are largely consistent with previous results but lay important groundwork to understand the effects of ligand substitution. We then turn to the hydride-substituted and halide-substituted clusters, comparing their geometries, electronic structures, and absorption spectra.

3.1. Unsubstituted $Au_9(PH_3)_8^{3+}$ and $Au_9(PPh_3)_8^{3+}$ nanoclusters

As mentioned in the Introduction, crystal structures of $Au_9(PR_3)_8^{3+}$ with both D_{4d} and D_{2h} symmetry have been observed;[62–64] previous theoretical work has focused on the structure with D_{2h} symmetry.[44,47] We have computed the properties of the NC structures with both symmetries, with both the simplified PH_3 ligands and the full PPh_3 ligands that are used experimentally. We focus first on the clusters with the simpler PH_3 ligands, then show that the cluster with the PPh_3

ligands has a similar electronic structure and a more complex absorption spectrum that is more similar to the experimental spectrum. The optimized $Au_9(PH_3)_8^{3+}$ structures with D_{4d} and D_{2h} symmetries are shown in **Figure 2a,d**. In both geometries, one Au atom is located in the center of the NC and is bound to eight peripheral Au atoms. At the revTPSS/TZP level with relativistic corrections, the structure with D_{4d} symmetry is 1.2 kcal/mol more stable than the structure with D_{2h} symmetry.

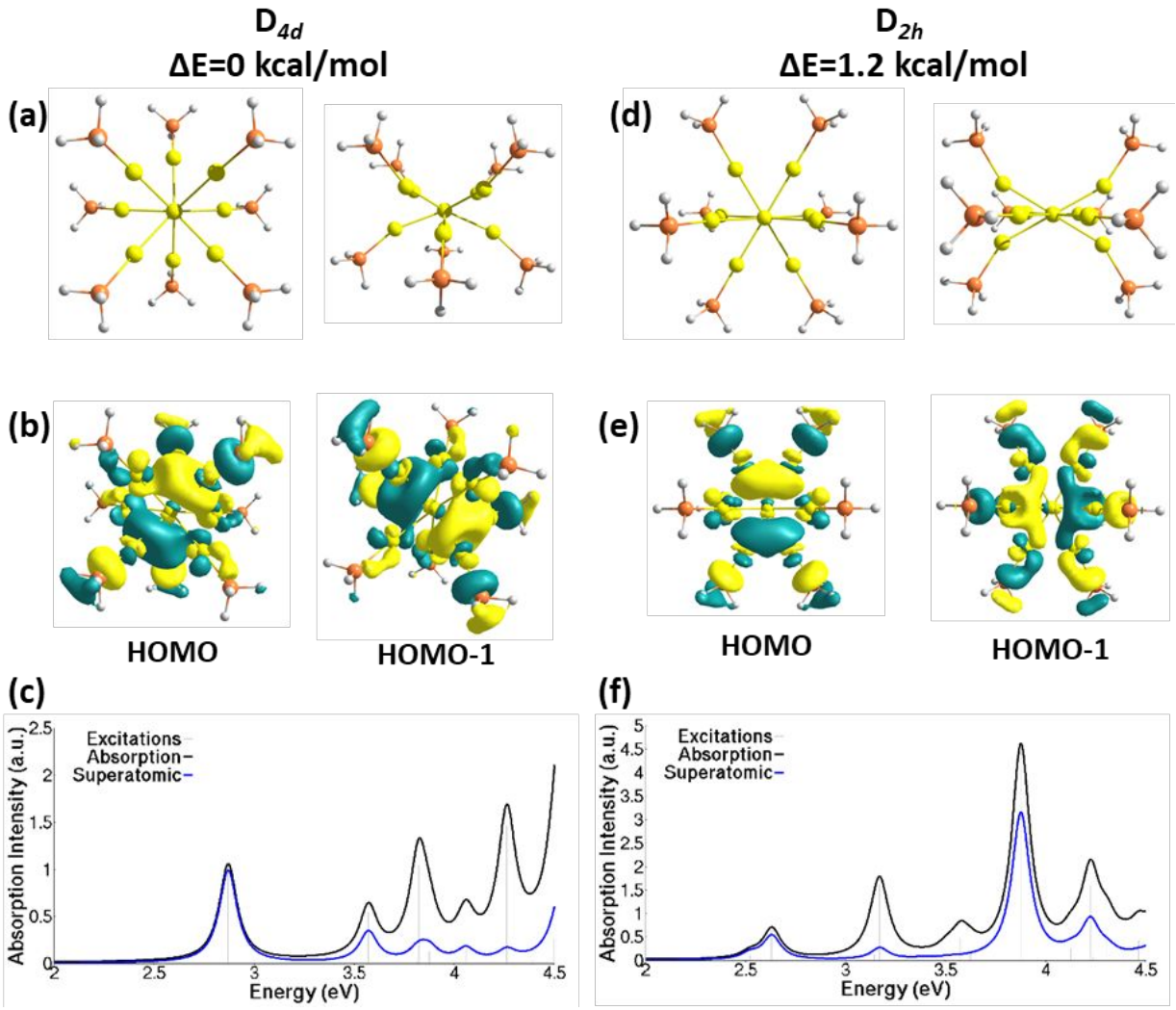

Figure 2. (a, d) Top and side views of the optimized geometries, (b, e) HOMO and HOMO-l superatomic orbitals, and (c, f) computed absorption spectra of the (a, b, c) D_{4d} and (d, e, f) D_{2h} structures of $Au_9(PH_3)_8^{3+}$.

In Au NCs, we can identify superatomic molecular orbitals (MOs), which are composed primarily of the Au 6s and 6p atomic orbitals and are delocalized across the Au core with shapes that resemble those of atomic orbitals.⁸²⁸¹[40] $Au_9(PR_3)_8^{3+}$ has been shown previously to have six electrons in superatomic orbitals,[44] with occupations of $1S^2 1P^4$. Our results are consistent, and the HOMO and HOMO-1 for both the D_{4d} and D_{2h} symmetries correspond to the $1P_y$ and $1P_x$ superatomic orbitals, respectively (**Figure 2b,e**). Because of the NC symmetry, the HOMO and HOMO-1 orbitals are degenerate for the D_{4d} structure but not for D_{2h}. For both structures, the $1P_z$ superatomic orbital aligned along the short axis of the NC is higher in energy that $1P_y$ and $1P_x$ superatomic orbitals because of the overall ellipsoidal NC shape, and is thus unoccupied. Mixing of the superatomic orbitals with the Au 5d orbitals and ligand-based orbitals makes distinguishing the 1S superatomic orbital difficult; thus, we focus here only on the 1P superatomic orbitals.

The computed absorption spectra for the two structures of the $Au_9(PH_3)_8^{3+}$ NC (**Figure 2c,f**) include several low-energy absorption peaks. The absorption spectra of the D_{2h} and D_{4d} structures are quite distinct, and both structures have significantly fewer low-energy absorption peaks than are visible in the experimental spectrum (**Figure 1a**). These differences are expected because it has been previously shown that the phenyl groups introduce many more absorption peaks below 3 eV.[44] Because the D_{2h} structure has fewer degenerate MOs, it exhibits more distinct absorption peaks than the D_{4d} structure. Our computed absorption spectrum for the D_{2h} structure is largely consistent with the previously computed spectrum,[44] with small blue shifts (about 0.3 eV) in the absorption energies because of differences in the functional used.

To understand the absorption spectra, we have also computed the contribution of the superatomic MOs to each excited state.[81] The low-lying unoccupied MOs of most Au NCs have significant superatomic character, so the analysis is based solely on the occupied MOs in each excited state. In the absorption spectrum of the D_{2h} structure, the peaks at 2.63 eV and 3.87 eV have primarily superatomic character (80% and 70%, respectively) involving excitations from the 1P superatomic orbitals. In contrast, the peaks at 3.17 eV and 3.57 eV have < 15% superatomic character. The peak at 3.17 eV primarily involves HOMO-2, and the peak at 3.57 eV is largely an excitation from HOMO-5 and HOMO-6; all of these MOs involve a combination of the Au 5d and ligand atomic orbitals. For the D_{4d} structure, the peak at 2.87 eV is 96% superatomic, and the somewhat weaker absorption peak at 3.57 eV has 61% superatomic character. The higher-energy absorption peaks have low superatomic character, indicating that they arise primarily from the Au 5d and ligand orbitals.

The $Au_9(PPh_3)_8^{3+}$ NC has two distinct local minima as shown in **Figure 3a,d**, similar to the structures with the simpler PH_3 ligands. However, the PPh_3 ligands reduce the symmetry, so the Au core only approximates D_{4d} and D_{2h} symmetry. At the revTPSS/TZP level, the structure with D_{2h}-like symmetry is 1.49 kcal/mol more stable than the structure with D_{4d}-like symmetry, which reverses the energetic ordering found for the PH_3 ligands. This highlights the importance of interactions between ligands in determining the relative stability of NC geometries. The electronic structures of the PPh_3-ligated NCs are consistent with the PH_3-ligated NCs, with the HOMO and HOMO-1 corresponding to the $1P_y$ and $1P_x$ superatomic orbitals (**Figure 3b,e**). In the structure with D_{2h}-like symmetry, the addition of the phenyl groups reduces the energy gap between the $1P_y$ and $1P_x$ superatomic orbitals from 0.77 eV to 0.59 eV. In contrast, in the structure with D_{4d}-like

symmetry, the phenyl groups break the degeneracy of the $1P_y$ and $1P_x$ superatomic orbitals and introduce an energy gap of 0.19 eV.

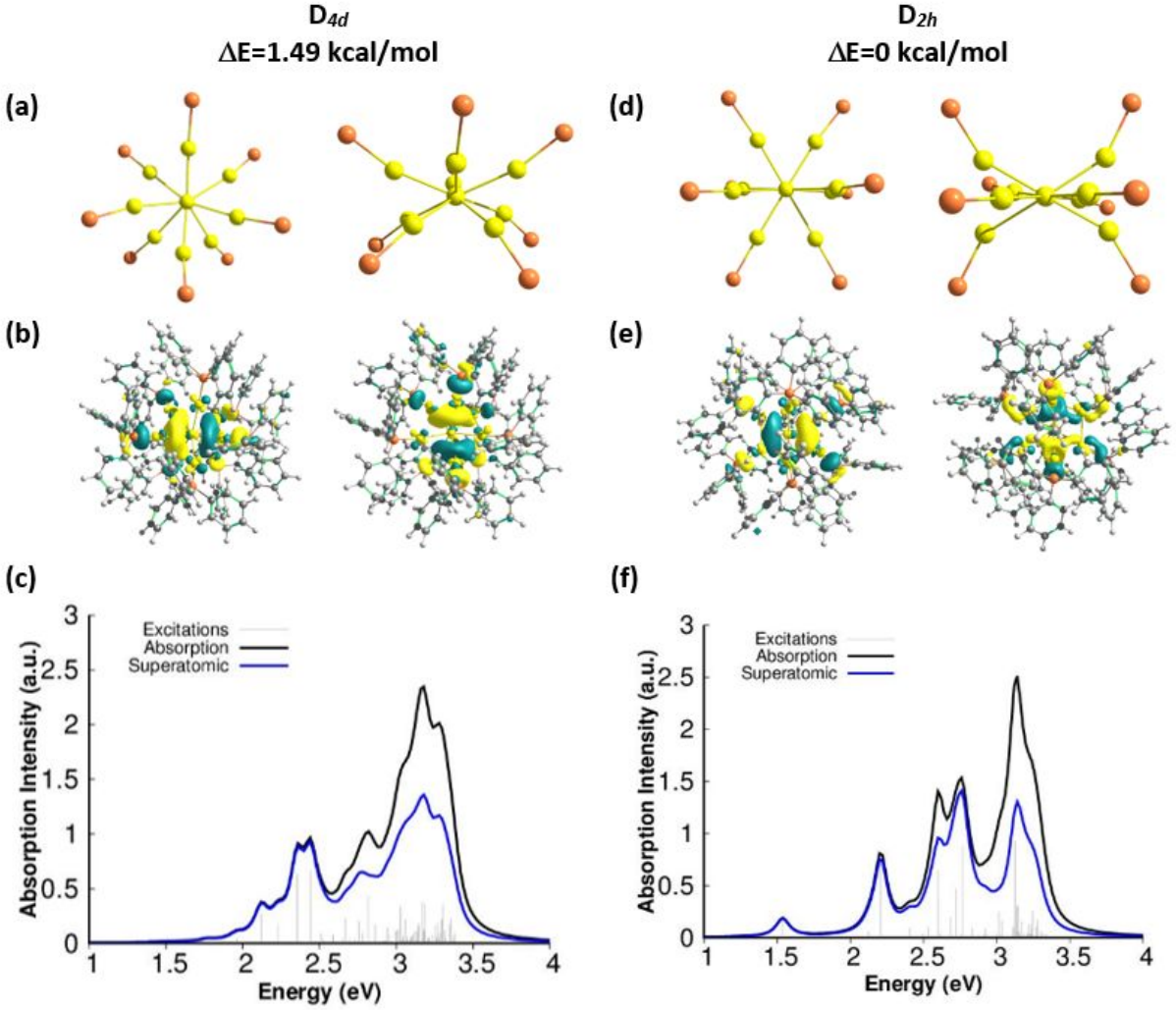

Figure 3. (a, d) Top and side views of the optimized geometries, (b, e) HOMO and HOMO-l superatomic orbitals, and (c, f) computed absorption spectra of the (a, b, c) D_{4d} and (d, e, f) D_{2h} structures of $Au_9(PPh_3)_8^{3+}$.

The computed absorption spectra for the two structures of the $Au_9(PPh_3)_8^{3+}$ NC are shown in **Figure 3c,f**; for reasons of computational cost, only excited states below ~3.4 eV could be computed. As has been shown previously,[44] addition of phenyl groups to the ligands introduces

many more absorption peaks below 3 eV. This is unsurprising because the phenyl groups shrink the HOMO-LUMO gap by 0.22 and 0.61 eV for the D_{2h}- and D_{4d}-like structures, respectively, with respect to the corresponding structures with PH_3 ligands. The NC with nearly D_{2h} symmetry has a small handful of excited states with relatively intense absorption, leading to the appearance of four relatively distinct absorption peaks between 2.2 and 3.2 eV. This is in fairly good agreement with the experimental spectrum (**Figure 1a**), which contains five distinct absorption peaks between 2.4 and 3.5 eV. The smaller number of peaks in our computed spectrum is likely due to the limited number of excited states that could be computed. In contrast, the NC with nearly D_{4d} symmetry has a much larger number of excited states with relatively comparable absorption intensity, leading to broader absorption with fewer distinct features. This suggests that the experimental absorption spectrum corresponds to NCs with nearly D_{2h} symmetry.

For the D_{2h}-like structure, most the absorption peaks below 2.77 eV have high superatomic character (90% to 100%), with the exception of the absorbing state at 2.60 eV with only 50% superatomic character; this excited state has 49% of its excitation from the HOMO-3 orbital. Above 2.77 eV, the superatomic character tends to decrease with increasing energy as the excited states gain more contributions from the occupied Au 5d and ligand orbitals. Similarly, for the D_{4d}-like structure, the absorption peaks below 2.59 eV are 98 to 100% superatomic, and the higher-energy states have lower superatomic character.

3.2. Hydride-substituted $Au_9(PH_3)_8H^{2+}$ and $Au_9(PPh_3)_8H^{2+}$ nanoclusters

To determine the most stable geometry of the hydride-substituted $Au_9(PH_3)_8H^{2+}$ NC, we used a two-step process. For initial screening, we constructed and optimized eleven different structures based on both the D_{2h} and D_{4d} structures of the unsubstituted NC, with the hydride ligand placed near either the central Au atom or near one or two of the outer Au atoms; these optimizations were performed at the BP86/DZ level. After removing duplicates in the optimized geometries, we selected all structures within 11.93 kcal/mol of the most stable structure for reoptimization at the revTPSS/TZP level; this functional has previously yielded accurate geometries and relative energies for Au NCs.[74] We focus here solely on the most stable geometry from this second optimization; this structure is 6.8 kcal/mol stable than any other structure, an order of magnitude larger than thermal energy at room temperature. More details on the higher-energy structures are available in the SI.

The most stable structure of $Au_9(PH_3)_8H^{2+}$ has the hydride ligand bonded directly to the low-coordination central atom of the Au_9 NC and has approximately C_{2v} symmetry (**Figure 4a**). Four of the outer Au atoms form a rectangle nearly co-planar with the central Au, and four are below that plane. This geometry is consistent with the previously published structure of this NC.[40] Notably, the alternation of Au atoms between upper and lower planes is much more similar to that of the unsubstituted D_{4d} structure than that of the unsubstituted D_{2h} cluster. In this geometry, the distance between the central Au atom and the hydride ligand is 0.19 Å shorter than the sum of the covalent radii[83] of the two atoms, and substantially shorter than the sum of the van der Waals radii (**Table 1**).[84] This suggests that the Au-H interaction involves strong orbital mixing, rather than the electron-withdrawing character typical of many anionic ligands. To enable more direct comparison to experimental results, we have also optimized $Au_9(PPh_3)_8H^{2+}$ with the full PPh_3 ligands used

experimentally (**Figure 4d**). The geometry of $Au_9(PPh_3)_8H^{2+}$ is quite similar to that of $Au_9(PH_3)_8H^{2+}$ and shows a 0.03 Å elongation of the Au-H bond, suggesting that the change in the ligands has minimal effects on the nature of the metal-ligand interaction. The binding of the hydride to both Au NCs is highly exothermic, with binding energies of 271.1 and 210.1 kcal/mol, respectively, for the NCs with PH_3 and PPh_3 ligands. This strong binding is unsurprising given the opposite charges of the two moieties.

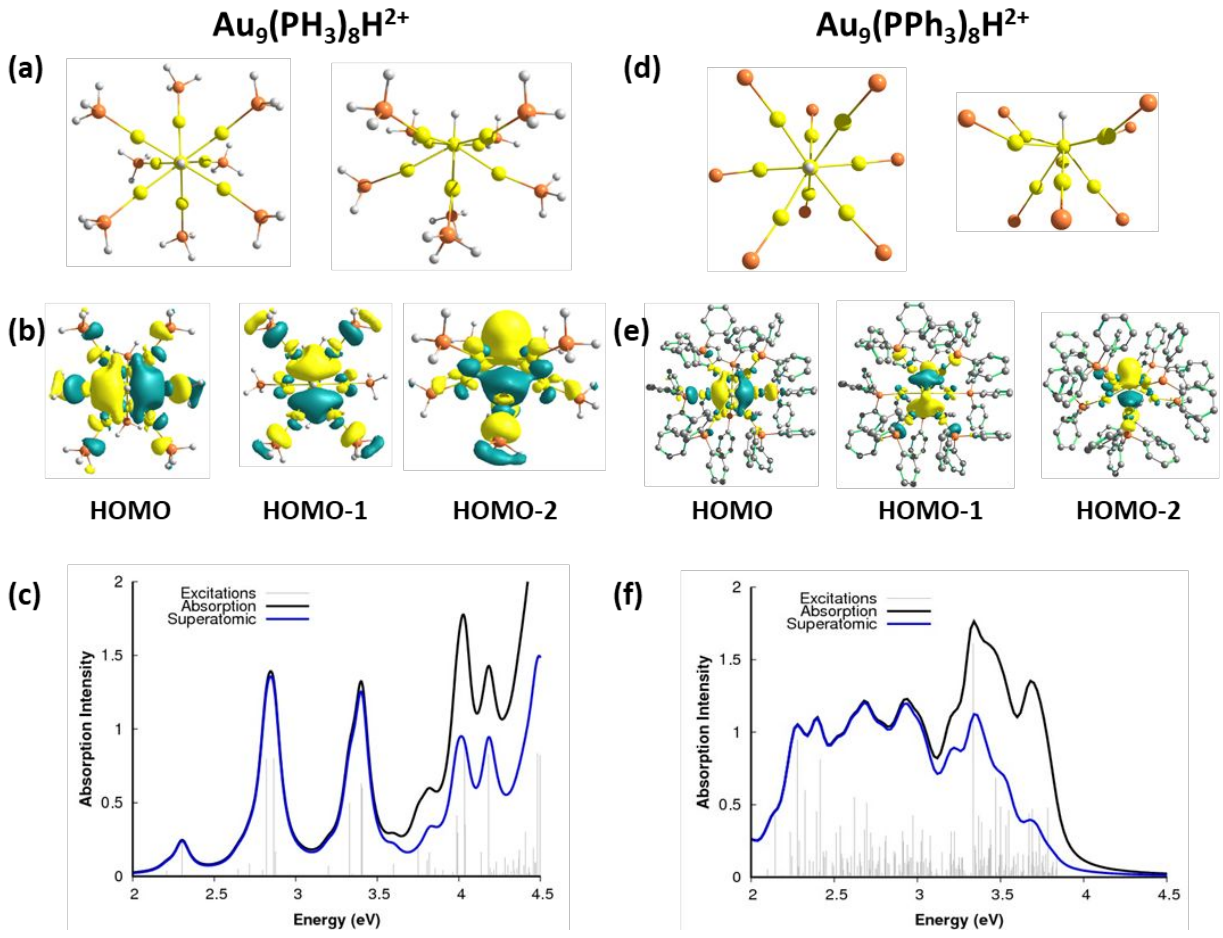

Figure 4. Optimized structures, (b, e) superatomic orbitals, and (c, f) absorption spectra of (a, b, c) $Au_9(PH_3)_8H^{2+}$ and (d, e, f) $Au_9(PPh_3)_8H^{2+}$. Ligands are excluded from panel d for clarity.

Table 1. PH_3- and PPh_3-protected Au-ligand (Au-L) interatomic distances ($d_{Au\text{-}L}$) and comparison to the sums of the van der Waals (ΣVDW) and covalent (ΣCovalent) radii of the two atoms. Au_a and Au_b indicate the two outer Au atoms closest to the ligand, and for the PPh_3-protected NCs, Au_c indicates the central Au atom.

Ligands	Au-L Bond	$d_{Au\text{-}L}$	$d_{Au\text{-}L} - \Sigma VDW$	$d_{Au\text{-}L} - \Sigma Covalent$
PH_3	Au_a-H	1.62	-1.24	-0.19
	Au_a-F	2.24	-0.89	0.09
	Au_b-F	2.57	-0.56	0.42
	Au_a-Cl	2.66	-0.75	0.23
	Au_b-Cl	2.67	-0.74	0.24
	Au_a-Br	2.75	-0.76	0.17
	Au_b-Br	2.76	-0.75	0.18
PPh_3	Au_a-H	1.65	-1.21	-0.16
	Au_a-F	2.46	-0.67	0.31
	Au_b-F	2.68	-0.45	0.53
	Au_c-F	2.60	-0.53	0.45
	Au_a-Cl	2.73	-0.68	0.30
	Au_b-Cl	3.86	0.45	1.43
	Au_c-Cl	3.44	0.03	1.01
	Au_a-Br	2.98	-0.53	0.40
	Au_b-Br	3.04	-0.47	0.46
	Au_c-Br	2.99	-0.52	0.41

The lack of electron-withdrawing character in the Au-H bond can be confirmed by examining the Hirshfeld atomic charges,[85] which have been commonly used to understand the electronic properties of Au NCs.[46,47,85,86] The Hirshfeld charges on both the hydride and attached central Au atom are close to zero (**Table 2**), which is unsurprising given that Au is slightly more electronegative than H (electronegativities of 2.54 and 2.20, respectively). These results are consistent with previous charge analyses of hydride-substituted Au NCs.[57] Replacement of the PH_3 ligands with PPh_3 ligands has minimal effects on the charge distribution, which is consistent with the small changes in the geometric structure.

Table 2. Hirshfeld charges for the hydride and halide ligands and the Au atoms bound to those ligands. Au_a and Au_b indicate the two outer Au atoms closest to the ligand, and for the PPh_3-protected NCs, Au_c indicates the central Au atom.

Ligands	Atom	H	F	Cl	Br
PH_3	Ligand	-0.082	-0.477	-0.314	-0.260
	Au_a	-0.003	0.043	-0.007	-0.013
	Au_b	-----	0.002	-0.007	-0.015
PPh_3	Ligand	-0.096	-0.468	-0.290	-0.261
	Au_a	-0.004	0.013	0.009	-0.025
	Au_b	-----	0.027	-0.040	-0.018
	Au_c	-----	-0.006	-0.034	-0.039

The hydride ligand substantially affects the electronic structure of $Au_9(PH_3)_8H^{2+}$ and produces a more isotropic structure. Unlike $Au_9(PH_3)_8^{3+}$, which has two occupied 1P superatomic orbitals, in $Au_9(PH_3)_8H^{2+}$ all three 1P superatomic orbitals are fully occupied and are relatively similar in energy. The orbital energy changes induced by the hydride ligand are large enough to cause a reordering of the superatomic orbital energies: in $Au_9(PH_3)_8H^{2+}$, the $1P_x$ and $1P_y$ superatomic orbitals (HOMO and HOMO-1) are higher in energy than the $1P_z$ superatomic orbital (HOMO-2) as shown in **Figure 4b**, which is a reversal the ordering seen in the unsubstituted NC. Thus, $Au_9(PH_3)_8H^{2+}$ can be viewed as a nearly spherical superatomic NC with a closed shell of eight superatomic electrons (1S not shown for the same reason given for the unsubstituted NC), consistent with previous computational results.[87] The Au−H bond has little effect on the $1P_x$ and $1P_y$ superatomic orbitals because of the NC symmetry, and both orbitals are composed primarily of the Au 6s and 6p atomic orbitals. The newly occupied $1P_z$ superatomic orbital is created mainly by a bonding interaction between the 6s orbital of the central Au atom and the 1s orbital of the hydride ligand and thus includes significant contributions from both the Au 6s and 6p orbitals and the H 1s orbital. As it is case for $Au_9(PH_3)_8H^{2+}$, $Au_9(PPh_3)_8H^{2+}$ also has three occupied 1P

superatomic orbitals (**Figure 4e**), and the $1P_z$ superatomic orbital is the lowest in energy of the three.

We have also computed the absorption spectra of both $Au_9(PH_3)_8H^{2+}$ (**Figure 4c**) and $Au_9(PPh_3)_8H^{2+}$ (**Figure 4f**) to determine the effect of the ligands on the absorption spectrum. $Au_9(PH_3)_8H^{2+}$ exhibits distinct absorption peaks near 2.8 and 3.4 eV, in contrast with the plateau in the experimental absorption spectrum between 2.5 and 3.3 eV (**Figure 1b**). The excited states below 3.5 eV are almost completely superatomic. The absorbing states at 2.3 eV and in the range of the 2.8 – 2.9 eV involve the $1P_x$ and $1P_y$ superatomic orbitals, whereas the absorbing states in the 3.3 – 3.4 eV range primarily involve the $1P_z$ superatomic orbital. The excited states above 3.5 eV have a mix of superatomic and ligand character. The computed absorption spectrum of $Au_9(PPh_3)_8H^{2+}$ (**Figure 4f**) is much more similar to the experimental absorption spectrum, with a plateau from 2.2 eV to 3.7 eV. For reasons of computational cost, excited states above 3.8 eV could not be computed. The inclusion of the full phenyl groups also introduces higher-energy occupied ligand MOs that reduce the energy at which the excited states switch from superatomic to ligand-based. The excited states below 3.1 eV have dominantly superatomic character; the excited states above 3.1 eV involve a mix of superatomic and ligand character. Overall, these results show that the experimental absorption spectrum of $Au_9(PPh_3)_8H^{2+}$ is consistent with the hydride ligand behaving as a metal dopant, and there is no evidence that the hydride ligand has electron-withdrawing character.

3.3. Halide-substituted $Au_9(PH_3)_8X^{2+}$ and $Au_9(PPh_3)_8X^{2+}$ nanoclusters

We now turn to the halide substituted NCs $Au_9(PH_3)_8X^{2+}$ and $Au_9(PPh_3)_8X^{2+}$, where X is F, Cl, or Br. The chloride- and bromide-substituted structures have been studied experimentally;[66] we also include the fluoride-substituted NC to extend the series. Our approach to determining the most stable structures of the halide-substituted NCs is similar to what we previously described for the hydride-substituted NCs. We constructed eleven different structures for each halide with the halide placed either near the center Au atom or near one or two of the outer Au atoms; structures were based on both the D_{2h} and D_{4d} structures of $Au_9(PH_3)_8^{3+}$. Several low-energy structures for each halide from our initial screening at the BP86/DZ level were re-optimized at the revTPSS/TZP level. The structures with PPh_3 ligands were optimized from structures based on the $Au_9(PH_3)_8X^{2+}$ minima.

Surprisingly, the most stable structures of the halide-substituted NCs are quite different from the geometry of the hydride-substituted NC, despite the strong similarities in the experimental absorption spectra. We have not found any stable geometries where the halide interacts directly with the central Au atom. In the most stable structures (**Figure 5**), the halide bridges two adjacent outer Au atoms. For the fluoride, chloride, and bromide ligands, these most stable structures are 8.1, 3.8, and 5.9 kcal/mol more stable than the second most stable structures, respectively. In all of these structures, the central Au atom is bonded only to the outer eight Au atoms and retains its low coordination. More details on the higher-energy structures are provided in the SI. All three halide ligands bind exothermically to the PH_3-protected Au NCs (232.5, 212.9 and 210.9 kcal/mol for fluoride, chloride, and bromide, respectively), though the binding is somewhat weaker than for the hydride clusters.

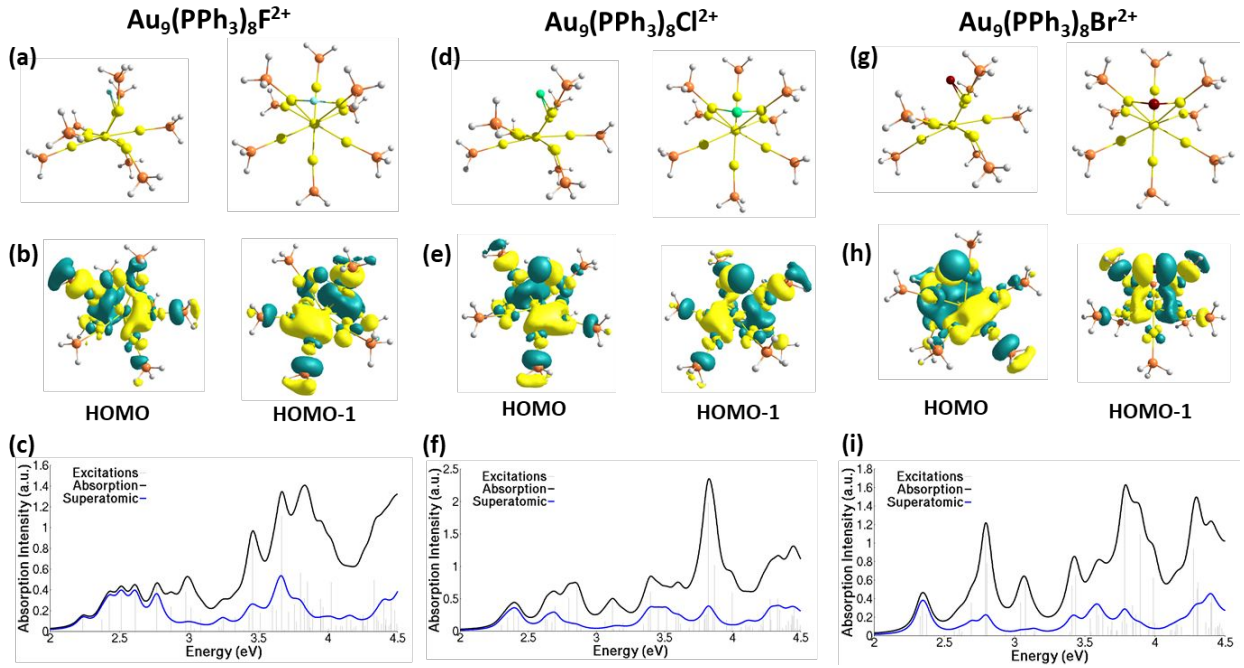

Figure 5. (a, d, g) Optimized structures, (b, e, h) superatomic orbitals, and (c, f, i) absorption spectra of (a, b, c) $Au_9(PH_3)_8F^{2+}$, (d, e, f) $Au_9(PH_3)_8Cl^{2+}$, and (g, h, i) $Au_9(PH_3)_8Br^{2+}$.

To understand the interactions of the halide ligands with the Au NC, we have analyzed the bond lengths and atomic charges, analogous to our exploration of the hydride ligand. The chloride and bromide ligands adsorb almost symmetrically, with two nearly equal Au-X bond lengths (**Table 1**). In contrast, the fluoride ligand adsorbs asymmetrically with one short and one long Au-F interaction. All Au-X interactions are significantly shorter than the sum of the van der Waals radii of the two atoms, but are longer than the sum of the covalent radii. This is in contrast with the Au-H bond, which is shorter than the sum of the covalent radii. These longer-distance interactions suggest that the Au-X interactions have significantly less covalent character than the Au-H interaction. The Hirshfeld atomic charges (**Table 2**) show substantial negative charge on all three halides, which is likewise in contrast with the extremely small negative charge on the hydride ligand. This suggests that the halide ligands all act as electron-withdrawing ligands, rather than

contributing their electrons to the Au NC as metal dopants. Since all three halides are significantly more electronegative than Au, it is unsurprising for these elements to have electron-withdrawing behavior. The electronic structure of the $Au_9(PH_3)_8X^{2+}$ NCs is also consistent with our assignment of the halide ligands as electron-withdrawing ligands. These NCs have two occupied 1P superatomic orbitals (HOMO, HOMO -1 in **Figure 5**) that are nearly degenerate; the halides do not introduce an additional occupied superatomic orbital, in contrast with the hydride ligand. To confirm that there is no occupied $1P_z$ superatomic MO, the HOMO-2 through HOMO-5 are shown in the SI (**Figures S7**, **S10**, and **S13**). In each case, three of these MOs have significant halide p character and one is clearly an Au d band MO; none of these MOs has $1P_z$ superatomic character. The superatomic orbitals have primarily Au 6s and 6p character but also include minor contributions from the halides, which increase with increasing halide size.

The optimized structures of the halide-substituted PPh_3-ligated NCs are distinctly different from the corresponding PH_3-ligated NCs and from each other; this result is in contrast with the strong similarities in the geometries of the PH_3- and PPh_3-ligated hydride-substituted NCs. The fluoride ligand binds asymmetrically such that it has a relatively short interactions with one outer Au atom and longer interactions with a second outer Au atom and the central Au atom; the shortest interaction is lengthened by 0.22 Å relative to the corresponding PH_3-ligated NC **(Table 1)**. The chloride ligand binds only to one outer Au atoms at a distance 0.07 Å longer than in the corresponding PH_3-ligated NC. However, since the chloride moves from a symmetric to an asymmetric binding site, its interactions with all other Au atoms occur at distances longer than the sum of the van der Waals radii. The bromide ligand maintains a nearly symmetric binding geometry, with interactions of nearly equal length with two outer Au atoms and the central Au

atom; the shortest interaction is lengthened by 0.23 Å relative to the corresponding PH_3-ligated NC. As in the case of the hydride-substituted clusters, the halide ligands bind somewhat more weakly to the PPh_3-ligated NCs, with binding energies of 165.8, 162.3 and 154.4 kcal/mol for fluoride, chloride, and bromide, respectively. Despite the geometric changes, the binding of the halides to the Au clusters is consistent with the ligands having electron-withdrawing character, rather than metal dopant character. The Hirshfeld charges (**Table 2**) on all three halides are significantly negative, and all halide-Au interactions are significantly longer than the sums of the covalent radii of the atoms. Similar to the corresponding PH_3-ligated NCs, the PPh_3-ligated halide-substituted NCs have only two occupied 1P superatomic orbitals (HOMO, HOMO -1 in **Figure 6**), in contrast with the hydride-substituted NC. The superatomic orbitals have primarily Au 6s and 6p character but also include minor contributions from the halides.

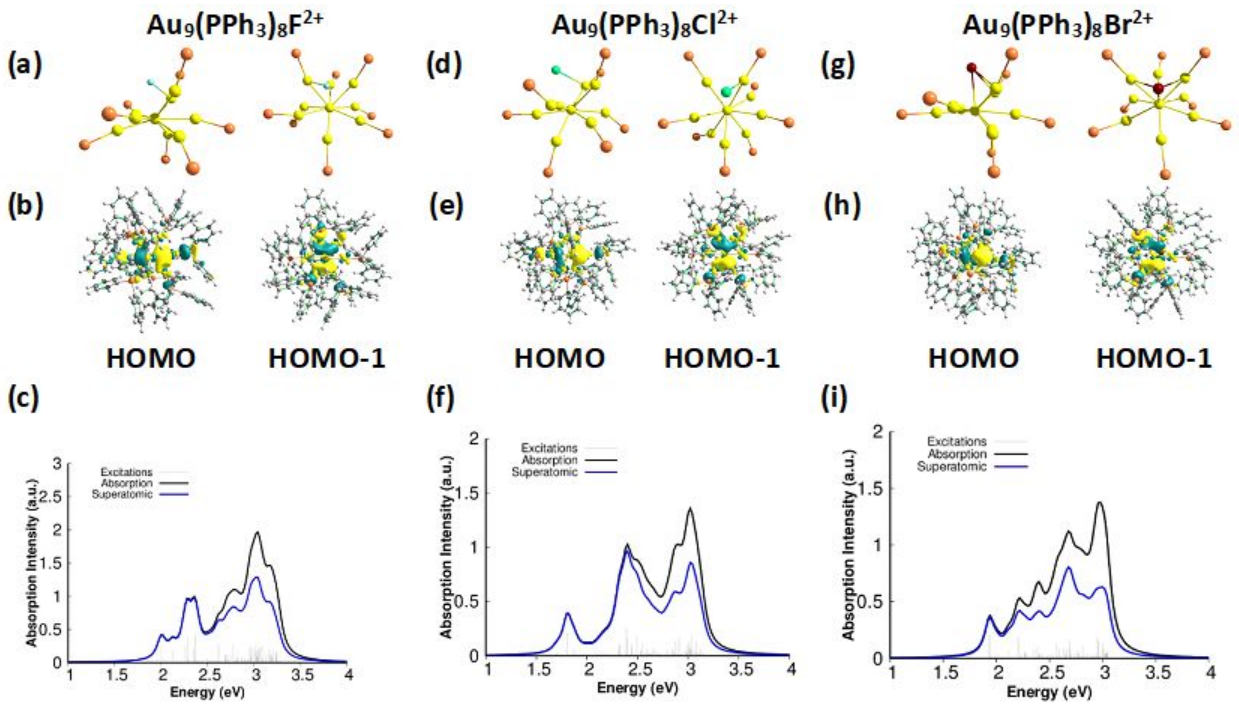

Figure 6. (a, d, g) Optimized structures, (b, e, h) superatomic orbitals, and (c, f, i) absorption spectra of (a, b, c) $Au_9(PPh_3)_8F^{2+}$, (d, e, f) $Au_9(PPh_3)_8Cl^{2+}$, and (g, h, i) $Au_9(PPh_3)_8Br^{2+}$.

The absorption spectra of the PH_3-ligated clusters include many absorption peaks. Because the halide-substituted NCs have one fewer occupied superatomic MO than the hydride-substituted NC, the excited states switch from mostly superatomic to mostly non-superatomic at lower energies. The excited states in the three halide-substituted NCs are superatomic only up to 2.5-2.7 eV, as compared to 3.5 eV for the hydride-substituted NC. The higher-energy excited states are mostly ligand-based. Among the halide-substituted NCs, the excited states of the fluoride-substituted NC have slightly more superatomic character than the chloride- and bromide-substituted NCs, which may be due to the smaller contributions of the fluoride atomic orbitals to the NC frontier MOs.

The computed absorption spectra of the PPh_3-ligated halide-substituted NCs (**Figure 6**) are in reasonable agreement with the experimental spectra (**Figure 1c,d**). As compared to the PH_3-ligated

NCs, the phenyl groups introduce additional low-energy excited states. Because the halide-substituted NCs have one fewer occupied superatomic MO than the hydride-substituted NC, the excited states switch to non-superatomic at lower energies for the halide-substituted NCs that the hydride-substituted NC.

Overall, these calculations demonstrate that the hydride- and halide-substituted Au_9 NCs have differences in their geometries and electronic structures. The halide ligands clearly act as electron-withdrawing ligands, in strong contrast to the metal dopant character of the hydride ligands. The similar experimental absorption spectra of the hydride- and halide-substituted Au_9 NCs are coincidental and disguise major differences in the geometries and electronic structures of these NCs. The halide ligands clearly act as electron-withdrawing ligands, in strong contrast to the metal dopant character of the hydride ligands.

4. Conclusions

Based on similarities in the experimental absorption spectra, it was recently proposed that hydride and halide substituents have similar binding modes with the $Au_9(PPh_3)_8^{3+}$ NC.[66] This proposal was in contrast with previous expectations that the hydride ligand would act as a metal dopant, whereas the halide ligands would have electron-withdrawing character. By computing the geometries and absorption spectra of the unsubstituted $Au_9(PH_3)_8^{3+}$ and $Au_9(PPh_3)_8^{3+}$ NCs and its hydride- and halide-substituted derivatives using DFT-based methods, we have shown that the hydride and

halide ligands have distinctly different binding geometries and electronic effects. The similarities in the experimental absorption spectra of these NCs disguise these substantial differences.

Consistent with previous DFT-based studies, we have showed that the hydride ligand in both $Au_9(PH_3)_8H^{2+}$ and $Au_9(PPh_3)_8H^{2+}$ binds to the central Au atom. The hydride ligand contributes its two electrons to the superatomic electron count, giving the NC one more occupied superatomic MO and a $1S^21P^6$ superatomic occupation. This is consistent with a description of the hydride ligand acting as a metal dopant. In contrast, the halide ligands bind in a position bridging two of the outer Au atoms for the PH_3-ligated NCs; in the PPh_3-ligated NCs, the halides have a larger variety of binding positions, but all involve relatively weak, long-distance interactions of the halides with the outer Au atoms. The halide ligands are electron-withdrawing and do not change the number of occupied superatomic orbitals, resulting in a $1S^21P^4$ superatomic occupation. Whereas the hydride ligand occupies a coordination site at the low-coordinated central Au atom, the halide ligands do not change the coordination of the central Au atom.

These results highlight the power of detailed theoretical analysis of the geometries and electronic structures of noble metal NCs to understand the role of ligands and interpret experimental data. In particular, they underline differences in the ability of ligands to modify the coordination environment of metal atoms, which is a feature that often correlates strongly with the catalytic activity of metal NCs. Understanding the roles of ligands in determining the properties of noble metal nanoclusters will support future efforts to use ligand derivatization as a powerful tool for the rational design of metal nanoclusters as efficient catalysts.

Acknowledgments

The authors thank Prof. Christopher Johnson for helpful discussion. This work was supported by start-up funding at Brandeis University. Computations were performed using Brandeis University's High Performance Computing Cluster, which is partially funded by DMR-MRSEC 1420382.

Supporting Information

Relative energies and absorption frames of studied clusters. Excited-state properties and Cartesian coordinates of the most stable bare and ligand-protected Au clusters.

References

(1) Schwerdtfeger, P. Gold Goes Nano - From Small Clusters to Low-Dimensional Assemblies. *Angew. Chemie - Int. Ed.* **2003**, *42* (17), 1892–1895. https://doi.org/10.1002/anie.200201610.

(2) Shang, L.; Dong, S.; Nienhaus, G. U. Ultra-Small Fluorescent Metal Nanoclusters: Synthesis and Biological Applications. *Nano Today* **2011**, *6* (4), 401–418. https://doi.org/10.1016/j.nantod.2011.06.004.

(3) Li, G.; Jin, R. Atomically Precise Gold Nanoclusters as New Model Catalysts. *Acc. Chem. Res.* **2013**, *46* (8), 1749–1758. https://doi.org/10.1021/ar300213z.

(4) Fang, J.; Zhang, B.; Yao, Q.; Yang, Y.; Xie, J.; Yan, N. Recent Advances in the Synthesis and Catalytic Applications of Ligand-Protected, Atomically Precise Metal Nanoclusters. *Coord. Chem. Rev.* **2016**, *322*, 1–29. https://doi.org/10.1016/j.ccr.2016.05.003.

(5) Zhao, J.; Ge, L.; Yuan, H.; Liu, Y.; Gui, Y.; Zhang, B.; Zhou, L.; Fang, S. Heterogeneous

Gold Catalysts for Selective Hydrogenation: From Nanoparticles to Atomically Precise Nanoclusters. *Nanoscale* **2019**, *11* (24), 11429–11436. https://doi.org/10.1039/C9NR03182K.

(6) Du, Y.; Sheng, H.; Astruc, D.; Zhu, M. Atomically Precise Noble Metal Nanoclusters as Efficient Catalysts: A Bridge between Structure and Properties. *Chem. Rev.* **2020**, *120* (2), 526–622. https://doi.org/10.1021/acs.chemrev.8b00726.

(7) Tian, S.; Cao, Y.; Chen, T.; Zang, S.; Xie, J. Ligand-Protected Atomically Precise Gold Nanoclusters as Model Catalysts for Oxidation Reactions. *Chem. Commun.* **2020**, *56* (8), 1163–1174. https://doi.org/10.1039/c9cc08215h.

(8) Liu, C.; Yan, C.; Lin, J.; Yu, C.; Huang, J.; Li, G. One-Pot Synthesis of Au 144 (SCH 2 Ph) 60 Nanoclusters and Their Catalytic Application. *J. Mater. Chem. A* **2015**, *3* (40), 20167–20173. https://doi.org/10.1039/C5TA05747G.

(9) Chen, H.; Liu, C.; Wang, M.; Zhang, C.; Luo, N.; Wang, Y.; Abroshan, H.; Li, G.; Wang, F. Visible Light Gold Nanocluster Photocatalyst: Selective Aerobic Oxidation of Amines to Imines. *ACS Catal.* **2017**, *7* (5), 3632–3638. https://doi.org/10.1021/acscatal.6b03509.

(10) Higaki, T.; Li, Q.; Zhou, M.; Zhao, S.; Li, Y.; Li, S.; Jin, R. Toward the Tailoring Chemistry of Metal Nanoclusters for Enhancing Functionalities. *Acc. Chem. Res.* **2018**, *51* (11), 2764–2773. https://doi.org/10.1021/acs.accounts.8b00383.

(11) Liu, C.; Ren, X.; Lin, F.; Fu, X.; Lin, X.; Li, T.; Sun, K.; Huang, J. Structure of the Au 23− x Ag x (S-Adm) 15 Nanocluster and Its Application for Photocatalytic Degradation of Organic Pollutants. *Angew. Chemie Int. Ed.* **2019**, *58* (33), 11335–11339. https://doi.org/10.1002/anie.201904612.

(12) Chai, O. J. H.; Liu, Z.; Chen, T.; Xie, J. Engineering Ultrasmall Metal Nanoclusters for

Photocatalytic and Electrocatalytic Applications. *Nanoscale* **2019**, *11* (43), 20437–20448. https://doi.org/10.1039/C9NR07272A.

(13) Qin, Z.; Zhao, D.; Zhao, L.; Xiao, Q.; Wu, T.; Zhang, J.; Wan, C.; Li, G. Tailoring the Stability, Photocatalysis and Photoluminescence Properties of Au11 Nanoclusters: Via Doping Engineering. *Nanoscale Adv.* **2019**, *1* (7), 2529–2536. https://doi.org/10.1039/c9na00234k.

(14) Jin, R. Quantum Sized, Thiolate-Protected Gold Nanoclusters. *Nanoscale* **2010**, *2* (3), 343–362. https://doi.org/10.1039/b9nr00160c.

(15) Qian, H.; Zhu, M.; Wu, Z.; Jin, R. Quantum Sized Gold Nanoclusters with Atomic Precision. *Acc. Chem. Res.* **2012**, *45* (9), 1470–1479. https://doi.org/10.1021/ar200331z.

(16) Negishi, Y.; Matsuura, Y.; Tomizawa, R.; Kurashige, W.; Niihori, Y.; Takayama, T.; Iwase, A.; Kudo, A. Controlled Loading of Small Aun Clusters (n = 10-39) onto BaLa4Ti4O15 Photocatalysts: Toward an Understanding of Size Effect of Cocatalyst on Water-Splitting Photocatalytic Activity. *J. Phys. Chem. C* **2015**, *119* (20), 11224–11232. https://doi.org/10.1021/jp5122432.

(17) Wang, Y.; Liu, X.; Wang, Q.; Quick, M.; Kovalenko, S.; Chen, Q.; Koch, N.; Pinna, N. Insights into Charge Transfer at the Atomically Precise Nanocluster/Semiconductor Interface for in-Depth Understanding the Role of Nanocluster in Photocatalytic System. *Angew. Chemie Int. Ed.* **2020**. https://doi.org/10.1002/anie.201915074.

(18) Abbas, M. A.; Kamat, P. V.; Bang, J. H. Thiolated Gold Nanoclusters for Light Energy Conversion. *ACS Energy Lett.* **2018**, *3* (4), 840–854. https://doi.org/10.1021/acsenergylett.8b00070.

(19) Li, G.; Jin, R. Gold Nanocluster-Catalyzed Semihydrogenation: A Unique Activation

Pathway for Terminal Alkynes. *J. Am. Chem. Soc.* **2014**, *136* (32), 11347–11354. https://doi.org/10.1021/ja503724j.

(20) Koklioti, M. A.; Skaltsas, T.; Sato, Y.; Suenaga, K.; Stergiou, A.; Tagmatarchis, N. Mechanistic Insights into the Photocatalytic Properties of Metal Nanocluster/Graphene Ensembles. Examining the Role of Visible Light in the Reduction of 4-Nitrophenol. *Nanoscale* **2017**, *9* (27), 9685–9692. https://doi.org/10.1039/C7NR02944F.

(21) Liu, C.; Abroshan, H.; Yan, C.; Li, G.; Haruta, M. One-Pot Synthesis of Au 11 (PPh 2 Py) 7 Br 3 for the Highly Chemoselective Hydrogenation of Nitrobenzaldehyde. *ACS Catal.* **2016**, *6* (1), 92–99. https://doi.org/10.1021/acscatal.5b02116.

(22) Xu, J.; Xu, S.; Chen, M.; Zhu, Y. Unlocking the Catalytic Activity of an Eight-Atom Gold Cluster with a Pd Atom. *Nanoscale* **2020**, *12* (10), 6020–6028. https://doi.org/10.1039/C9NR10198E.

(23) Jin, R.; Li, G.; Sharma, S.; Li, Y.; Du, X. Toward Active-Site Tailoring in Heterogeneous Catalysis by Atomically Precise Metal Nanoclusters with Crystallographic Structures. *Chem. Rev.* **2020**, acs.chemrev.0c00495. https://doi.org/10.1021/acs.chemrev.0c00495.

(24) Cai, X.; Saranya, G.; Shen, K.; Chen, M.; Si, R.; Ding, W.; Zhu, Y. Reversible Switching of Catalytic Activity by Shuttling an Atom into and out of Gold Nanoclusters. *Angew. Chemie Int. Ed.* **2019**, *58* (29), 9964–9968. https://doi.org/10.1002/anie.201903853.

(25) Liu, Y.; Chai, X.; Cai, X.; Chen, M.; Jin, R.; Ding, W.; Zhu, Y. Central Doping of a Foreign Atom into the Silver Cluster for Catalytic Conversion of CO 2 toward C−C Bond Formation. *Angew. Chemie Int. Ed.* **2018**, *57* (31), 9775–9779. https://doi.org/10.1002/anie.201805319.

(26) Choi, W.; Hu, G.; Kwak, K.; Kim, M.; Jiang, D.; Choi, J.-P.; Lee, D. Effects of Metal-Doping on Hydrogen Evolution Reaction Catalyzed by MAu 24 and M 2 Au 36

Nanoclusters (M = Pt, Pd). *ACS Appl. Mater. Interfaces* **2018**, *10* (51), 44645–44653. https://doi.org/10.1021/acsami.8b16178.

(27) Jin, R.; Zeng, C.; Zhou, M.; Chen, Y. Atomically Precise Colloidal Metal Nanoclusters and Nanoparticles: Fundamentals and Opportunities. *Chem. Rev.* **2016**, *116* (18), 10346–10413. https://doi.org/10.1021/acs.chemrev.5b00703.

(28) Liu, P.; Qin, R.; Fu, G.; Zheng, N. Surface Coordination Chemistry of Metal Nanomaterials. *J. Am. Chem. Soc.* **2017**, *139* (6), 2122–2131. https://doi.org/10.1021/jacs.6b10978.

(29) Li, G.; Abroshan, H.; Liu, C.; Zhuo, S.; Li, Z.; Xie, Y.; Kim, H. J.; Rosi, N. L.; Jin, R. Tailoring the Electronic and Catalytic Properties of Au 25 Nanoclusters via Ligand Engineering. *ACS Nano* **2016**, *10* (8), 7998–8005. https://doi.org/10.1021/acsnano.6b03964.

(30) Wan, X.-K.; Wang, J.-Q.; Nan, Z.-A.; Wang, Q.-M. Ligand Effects in Catalysis by Atomically Precise Gold Nanoclusters. *Sci. Adv.* **2017**, *3* (10), e1701823. https://doi.org/10.1126/sciadv.1701823.

(31) Higaki, T.; Li, Y.; Zhao, S.; Li, Q.; Li, S.; Du, X.; Yang, S.; Chai, J.; Jin, R. Atomically Tailored Gold Nanoclusters for Catalytic Application. *Angew. Chemie Int. Ed.* **2019**, *58* (25), 8291–8302. https://doi.org/10.1002/anie.201814156.

(32) Nasaruddin, R. R.; Chen, T.; Li, J.; Goswami, N.; Zhang, J.; Yan, N.; Xie, J. Ligands Modulate Reaction Pathway in the Hydrogenation of 4-Nitrophenol Catalyzed by Gold Nanoclusters. *ChemCatChem* **2018**, *10* (2), 395–402. https://doi.org/10.1002/cctc.201701472.

(33) Yuan, S.-F.; Lei, Z.; Guan, Z.-J.; Wang, Q.-M. Atomically Precise Preorganization of Open Metal Sites on Gold Nanocluster with High Catalytic Performance. *Angew. Chemie Int. Ed.*

2020, anie.202012499. https://doi.org/10.1002/anie.202012499.

(34) Zhao, S.; Austin, N.; Li, M.; Song, Y.; House, S. D.; Bernhard, S.; Yang, J. C.; Mpourmpakis, G.; Jin, R. Influence of Atomic-Level Morphology on Catalysis: The Case of Sphere and Rod-Like Gold Nanoclusters for CO 2 Electroreduction. *ACS Catal.* **2018**, *8* (6), 4996–5001. https://doi.org/10.1021/acscatal.8b00365.

(35) Goel, S.; Velizhanin, K. A.; Piryatinski, A.; Ivanov, S. A.; Tretiak, S. Ligand Effects on Optical Properties of Small Gold Clusters: A TDDFT Study. *J. Phys. Chem. C* **2012**, *116* (5), 3242–3249. https://doi.org/10.1021/jp208732k.

(36) Goel, S.; Velizhanin, K. A.; Piryatinski, A.; Tretiak, S.; Ivanov, S. A. DFT Study of Ligand Binding to Small Gold Clusters. *J. Phys. Chem. Lett.* **2010**, *1* (6), 927–931. https://doi.org/10.1021/jz1000193.

(37) Shabaninezhad, M.; Abuhagr, A.; Sakthivel, N. A.; Kumara, C.; Dass, A.; Kwak, K.; Pyo, K.; Lee, D.; Ramakrishna, G. Ultrafast Electron Dynamics in Thiolate-Protected Plasmonic Gold Clusters: Size and Ligand Effect. *J. Phys. Chem. C* **2019**, *123* (21), 13344–13353. https://doi.org/10.1021/acs.jpcc.9b01739.

(38) Johnson, G. E.; Laskin, J. Understanding Ligand Effects in Gold Clusters Using Mass Spectrometry. *Analyst* **2016**, *141* (12), 3573–3589. https://doi.org/10.1039/c6an00263c.

(39) Günter Schmid, Benedetto Corain, N. T. *Metal Nanoclusters in Catalysis and Materials Science: The Issue of Size Control*; Elsevier Ltd, 2011.

(40) Walter, M.; Akola, J.; Lopez-Acevedo, O.; Jadzinsky, P. D.; Calero, G.; Ackerson, C. J.; Whetten, R. L.; Gronbeck, H.; Hakkinen, H. A Unified View of Ligand-Protected Gold Clusters as Superatom Complexes. *Proc. Natl. Acad. Sci. USA* **2008**, *105*, 9157–9162. https://doi.org/10.1073/pnas.0801001105.

(41) Häkkinen, H. Electronic Shell Structures in Bare and Protected Metal Nanoclusters. *Adv. Phys. X* **2016**, *1* (3), 467–491. https://doi.org/10.1080/23746149.2016.1219234.

(42) Lopez-Acevedo, O.; Akola, J.; Whetten, R. L.; Grönbeck, H.; Häkkinen, H. Structure and Bonding in the Ubiquitous Icosahedral Metallic Gold Cluster Au 144(SR) 60. *J. Phys. Chem. C* **2009**, *113* (13), 5035–5038. https://doi.org/10.1021/jp8115098.

(43) Lugo, G.; Schwanen, V.; Fresch, B.; Remacle, F. Charge Redistribution Effects on the UV-Vis Spectra of Small Ligated Gold Clusters: A Computational Study. *J. Phys. Chem. C* **2015**, *119* (20), 10969–10980. https://doi.org/10.1021/jp511120j.

(44) Karimova, N. V.; Aikens, C. M. Time Dependent Density Functional Theory Study of Magnetic Circular Dichroism Spectra of Gold Clusters Au 9 (PH 3) 8 3+ and Au 9 (PPh 3) 8 3+ . *J. Phys. Chem. A* **2016**, *120* (48), 9625–9635. https://doi.org/10.1021/acs.jpca.6b10063.

(45) Karimova, N. V.; Aikens, C. M. Optical Properties of Small Gold Clusters Au8L82+ (L = PH3, PPh3): Magnetic Circular Dichroism Spectra. *J. Phys. Chem. C* **2017**, *121* (35), 19478–19489. https://doi.org/10.1021/acs.jpcc.7b05630.

(46) Weerawardene, K. L. D. M.; Aikens, C. M. Theoretical Insights into the Origin of Photoluminescence of Au25(SR)18- Nanoparticles. *J. Am. Chem. Soc.* **2016**, *138* (35), 11202–11210. https://doi.org/10.1021/jacs.6b05293.

(47) Muniz-Miranda, F.; Menziani, M. C.; Pedone, A. Assessment of Exchange-Correlation Functionals in Reproducing the Structure and Optical Gap of Organic-Protected Gold Nanoclusters. *J. Phys. Chem. C* **2014**, *118* (14), 7532–7544. https://doi.org/10.1021/jp411483x.

(48) Muñoz-Castro, A. On the Ligand-Core Interaction in Ligand-Protected Gold Superatoms.

Insights from Au25(XR)18 (X = S, Se, Te): Via Relativistic DFT Calculations. *Phys. Chem. Chem. Phys.* **2019**, *21* (24), 13022–13029. https://doi.org/10.1039/c9cp02077b.

(49) Mingos, D. M. P. Structural and Bonding Patterns in Gold Clusters. *Dalt. Trans.* **2015**, *44* (15), 6680–6695. https://doi.org/10.1039/c5dt00253b.

(50) Zhu, M.; Aikens, C. M.; Hendrich, M. P.; Gupta, R.; Qian, H.; Schatz, G. C.; Jin, R. Reversible Switching of Magnetism in Thiolate-Protected Au 25 Superatoms. *J. Am. Chem. Soc.* **2009**, *131* (7), 2490–2492. https://doi.org/10.1021/ja809157f.

(51) Kwak, K.; Choi, W.; Tang, Q.; Jiang, D.; Lee, D. Rationally Designed Metal Nanocluster for Electrocatalytic Hydrogen Production from Water. *J. Mater. Chem. A* **2018**, *6* (40), 19495–19501. https://doi.org/10.1039/C8TA06306K.

(52) Hu, G.; Wu, Z.; Jiang, D. Stronger-than-Pt Hydrogen Adsorption in a Au 22 Nanocluster for the Hydrogen Evolution Reaction. *J. Mater. Chem. A* **2018**, *6* (17), 7532–7537. https://doi.org/10.1039/C8TA00461G.

(53) Buckart, S.; Ganteför, G.; Kim, Y. D.; Jena, P. Anomalous Behavior of Atomic Hydrogen Interacting with Gold Clusters. *J. Am. Chem. Soc.* **2003**, *125* (46), 14205–14209. https://doi.org/10.1021/ja036544t.

(54) Mondal, K.; Agrawal, S.; Manna, D.; Banerjee, A.; Ghanty, T. K. Effect of Hydrogen Atom Doping on the Structure and Electronic Properties of 20-Atom Gold Cluster. *J. Phys. Chem. C* **2016**, *120* (33), 18588–18594. https://doi.org/10.1021/acs.jpcc.6b04584.

(55) Takano, S.; Hirai, H.; Muramatsu, S.; Tsukuda, T. Hydride-Doped Gold Superatom (Au 9 H) 2+ : Synthesis, Structure, and Transformation. *J. Am. Chem. Soc.* **2018**, *140* (27), 8380–8383. https://doi.org/10.1021/jacs.8b03880.

(56) Takano, S.; Hasegawa, S.; Suyama, M.; Tsukuda, T. Hydride Doping of Chemically

Modified Gold-Based Superatoms. *Acc. Chem. Res.* **2018**, *51* (12), 3074–3083. https://doi.org/10.1021/acs.accounts.8b00399.

(57) Hu, G.; Tang, Q.; Lee, D.; Wu, Z.; Jiang, D. E. Metallic Hydrogen in Atomically Precise Gold Nanoclusters. *Chem. Mater.* **2017**, *29* (11), 4840–4847. https://doi.org/10.1021/acs.chemmater.7b00776.

(58) Hirai, H.; Takano, S.; Tsukuda, T. Synthesis of Trimetallic (HPd@M 2 Au 8) 3+ Superatoms (M = Ag, Cu) via Hydride-Mediated Regioselective Doping to (Pd@Au 8) 2+. *ACS Omega* **2019**, *4* (4), 7070–7075. https://doi.org/10.1021/acsomega.9b00575.

(59) Cariati, F.; Naldini, L. Preparation and Properties of Gold Atom Cluster Compounds : Octakis- (Triary1phosphine)Enneagold Trianion. *J.C.S. Dalt.* **1972**, *20*, 2286–2287.

(60) Takano, S.; Yamazoe, S.; Tsukuda, T. A Gold Superatom with 10 Electrons in Au13(PPh3)8(p-SC6H4CO2H)3. *APL Mater.* **2017**, *5* (5), 3–8. https://doi.org/10.1063/1.4976018.

(61) Das, A.; Liu, C.; Byun, H. Y.; Nobusada, K.; Zhao, S.; Rosi, N.; Jin, R. Structure Determination of [Au18(SR)14]. *Angew. Chemie - Int. Ed.* **2015**, *54* (10), 3140–3144. https://doi.org/10.1002/anie.201410161.

(62) Hall, K. P.; Theoblad, B. R. C.; Gilmour, D. I.; Mingos, D. M. P.; Welch, A. J. Synthesis and Structural Characterization of [Au9{P(p-C6H4OMe)3}8](BF4)3; a Cluster with a Centred Crown of Gold Atoms. *J. Chem. Soc. Chem. Commun.* **1982**, *3* (10), 528. https://doi.org/10.1039/c39820000528.

(63) Schulz-Dobrick, M.; Jansen, M. Supramolecular Intercluster Compounds Consisting of Gold Clusters and Keggin Anions. *Eur. J. Inorg. Chem.* **2006**, *2006* (22), 4498–4502. https://doi.org/10.1002/ejic.200600790.

(64) Wen, F.; Englert, U.; Gutrath, B.; Simon, U. Crystal Structure, Electrochemical and Optical Properties of [Au 9(PPh3)8](NO3)3. *Eur. J. Inorg. Chem.* **2008**, *9* (1), 106–111. https://doi.org/10.1002/ejic.200700534.

(65) Hirata, K.; Chakraborty, P.; Nag, A.; Takano, S.; Koyasu, K.; Pradeep, T.; Tsukuda, T. Interconversions of Structural Isomers of [PdAu 8 (PPh 3) 8] 2+ and [Au 9 (PPh 3) 8] 3+ Revealed by Ion Mobility Mass Spectrometry. *J. Phys. Chem. C* **2018**, *122* (40), 23123–23128. https://doi.org/10.1021/acs.jpcc.8b04722.

(66) Cirri, A.; Hernández, H. M.; Johnson, C. J. Hydride, Chloride, and Bromide Show Similar Electronic Effects in the Au9(PPh3)83+ Nanocluster. *Chem. Commun.* **2020**, *56* (8), 1283–1285. https://doi.org/10.1039/c9cc08009k.

(67) Becke, A. D. Density-Functional Exchange-Energy Approximation with Correct Asymptotic Behavior. *Phys. Rev. A* **1988**, *38*, 3098–3100. https://doi.org/10.1103/PhysRevA.38.3098.

(68) Perdew, J. P. Density-Functional Approximation for the Correlation Energy of the Inhomogeneous Electron Gas. *Phys. Rev. B* **1986**, *33*, 8822–8824. https://doi.org/10.1103/PhysRevB.33.8822.

(69) Aikens, C. M.; Schatz, G. C. TDDFT Studies of Absorption and SERS Spectra of Pyridine Interacting with Au20. *J. Phys. Chem. A* **2006**, *110*, 13317–13324.

(70) Fihey, A.; Kloss, B.; Perrier, A.; Maurel, F. Density Functional Theory Study of the Conformation and Optical Properties of Hybrid Au(n)-Dithienylethene Systems (n = 3, 19, 25). *J. Phys. Chem. A* **2014**, *118* (26), 4695–4706. https://doi.org/10.1021/jp501542m.

(71) Bae, G.; Aikens, C. M. Time-Dependent Density Functional Theory Studies of Optical Properties of Au Nanoparticles: Octahedra, Truncated Octahedra, and Icosahedra. *J. Phys.*

Chem. C **2015**, *119*, 23127−23137. https://doi.org/10.1021/jp300789x.

(72) Chen, L.; Gao, Y.; Cheng, Y.; Li, H.; Wang, Z.; Li, Z.; Zhang, R.-Q. Nonresonant Chemical Mechanism in Surface-Enhanced Raman Scattering of Pyridine on M@Au 12 Clusters. *Nanoscale* **2016**, *8*, 4086–4093. https://doi.org/10.1039/C5NR07246H.

(73) Perdew, J. P.; Ruzsinszky, A.; Csonka, G. I.; Constantin, L. A.; Sun, J. Workhorse Semilocal Density Functional for Condensed Matter Physics and Quantum Chemistry. *Phys. Rev. Lett.* **2009**, *103* (2), 10–13. https://doi.org/10.1103/PhysRevLett.103.026403.

(74) Baek, H.; Moon, J.; Kim, J. Benchmark Study of Density Functional Theory for Neutral Gold Clusters, Aun (n = 2-8). *J. Phys. Chem. A* **2017**, *121* (12), 2410–2419. https://doi.org/10.1021/acs.jpca.6b11868.

(75) Gritsenko, O. V; Schipper, P. R. T.; Baerends, E. J. Approximation of the Exchange-Correlation Kohn–Sham Potential with a Statistical Average of Different Orbital Model Potentials. *Chem. Phys. Lett.* **1999**, *302*, 199–207.

(76) van Lenthe, E.; Snijders, J. G.; Baerends, E. J. The Zero-Order Regular Approximation for Relativistic Effects: The Effect of Spin–Orbit Coupling in Closed Shell Molecules. *J. Chem. Phys.* **1996**, *105*, 6505–6516.

(77) Jiang, D. E.; Kühn, M.; Tang, Q.; Weigend, F. Superatomic Orbitals under Spin-Orbit Coupling. *J. Phys. Chem. Lett.* **2014**, *5* (19), 3286–3289. https://doi.org/10.1021/jz501745z.

(78) Yuan, H. K.; Chen, H.; Kuang, A. L.; Wu, B.; Wang, J. Z. Structural and Magnetic Properties of Small 4d Transition Metal Clusters: Role of Spin-Orbit Coupling. *J. Phys. Chem. A* **2012**, *116* (47), 11673–11684. https://doi.org/10.1021/jp307202t.

(79) te Velde, G.; Bickelhaupt, F. M.; Baerends, E. J.; Fonseca Guerra, C.; van Gisbergen, S. J. A. A.; Snijders, J. G.; Ziegler, T. Chemistry with ADF. *J. Comput. Chem.* **2000**, *22* (9),

931–967. https://doi.org/10.1002/jcc.1056.

(80) Amsterdam Density Functional 2018; SCM, Theoretical Chemistry: Vrije Universiteit, Amsterdam, The Netherlands.

(81) Gieseking, R. L. M.; Ashwell, A. P.; Ratner, M. A.; Schatz, G. C. Analytical Approaches To Identify Plasmon-like Excited States in Bare and Ligand-Protected Metal Nanoclusters. *J. Phys. Chem. C* **2020**, *124* (5), 3260–3269. https://doi.org/10.1021/acs.jpcc.9b10569.

(82) Segala, M.; Schneider, F. S. S.; Caramori, G. F.; Parreira, R. L. T. Evaluation of Electron Donation as a Mechanism for the Stabilisation of Chalcogenate-Protected Gold Nanoclusters. *ChemPhysChem* **2016**, *17* (19), 3102–3111. https://doi.org/10.1002/cphc.201600552.

(83) Sanderson, R. T. Electronegativity and Bond Energy. *J. Am. Chem. Soc.* **1983**, *105* (8), 2259–2261. https://doi.org/10.1021/ja00346a026.

(84) Bondi, A. Van Der Waals Volumes and Radii. *J. Phys. Chem.* **1964**, *68*, 441–451.

(85) Hirshfeld, F. L. Bonded-Atom Fragments for Describing Molecular Charge Densities. *Theor. Chim. Acta* **1977**, *44*, 129–138. https://doi.org/10.1007/BF00549096.

(86) Muniz-Miranda, F.; Presti, D.; Menziani, M. C.; Pedone, A. Electronic and Optical Properties of the Au22[1,8-Bis(Diphenylphosphino) Octane]6 Nanoclusters Disclosed by DFT and TD-DFT Calculations. *Theor. Chem. Acc.* **2016**, *135* (1), 1–9. https://doi.org/10.1007/s00214-015-1764-x.

(87) Omoda, T.; Takano, S.; Tsukuda, T. Toward Controlling the Electronic Structures of Chemically Modified Superatoms of Gold and Silver. *Small* **2020**, *2001439*, 1–18. https://doi.org/10.1002/smll.202001439.